

# Dependence of Catalytic Activity of Nanocrystalline Nickel Ferrite on Its Structural, Morphological, Optical, and Magnetic Properties in Aerobic Oxidation of Benzyl Alcohol

R. Saranya<sup>1</sup> · R. Azhagu Raj<sup>2,3</sup> · M. S. AlSalhi<sup>4,5</sup> · S. Devanesan<sup>4,5</sup>

Received: 9 June 2017 / Accepted: 19 August 2017 / Published online: 31 August 2017  
© Springer Science+Business Media, LLC 2017

**Abstract** Nanocrystalline nickel ferrite spinel,  $\text{NiFe}_2\text{O}_4$ , with average crystallite size of 23.98 and 19.76 nm were successfully synthesized under sol–gel method (SGM) and microwave method (MM) conditions without using any surfactant or otherwise structure-directing (oxalic acid as the fuel) agents. Powder x-ray diffraction, high-resolution scanning electron microscopies indicate that single-crystalline nanoparticles are well-dispersed in the nickel ferrite. The elemental investigation of nickel ferrite was attained from energy-dispersive x-ray (EDX) analysis. Their optical properties (diffuse reflectance spectroscopy and photoluminescence) were described in depth in relative with their structural characteristics and the functionalization performance. After the magnetic measurements, samples showed

a ferromagnetic behavior and the magnetization ( $M_s$ ) value of  $\text{NiFe}_2\text{O}_4$ -MM is higher, i.e., 59.33 emu/g than  $\text{NiFe}_2\text{O}_4$ -SGM (50.12 emu/g). The magnetic properties could be further changed by controlling the shape, size, and crystallinity of the nanocrystals. Determination of concentration  $\text{NiFe}_2\text{O}_4$  ions' average number of atoms per nanoparticle was calculated by the new method as follows. Consequently, the designated procedure improves catalytic activity of nickel ferrite powders in aerobic oxidation of benzyl alcohol and catalytic reactions.

**Keywords** Nickel ferrite spinel · Nanocatalyst · Sol–gel and microwave method · Aerobic oxidation · X-ray diffraction · Electron microscopy

✉ R. Azhagu Raj  
drazhaguraj@gmail.com

✉ M. S. AlSalhi  
malsalhy@gmail.com

<sup>1</sup> Department of Science and Humanities, M. Kumarasamy College of Engineering, Karur, Tamil Nadu, India

<sup>2</sup> Department of Animal Science, Manonmaniam Sundaranar University, Tirunelveli, Tamil Nadu 627012, India

<sup>3</sup> Department of Zoology, St. Xavier's College (Autonomous), Palayamkottai, Tamil Nadu 627002, India

<sup>4</sup> Research Chair in Laser Diagnosis of Cancers, Department of Physics and Astronomy, College of Science, King Saud University, Riyadh, Saudi Arabia

<sup>5</sup> Department of Physics and Astronomy, College of Science, King Saud University, Riyadh, Saudi Arabia

## 1 Introduction

The structural, morphological, optical, and magnetic properties of nanomaterials have been increasingly controlled by their methods of synthesis, primarily because of the relationship between the shapes and the properties of metal oxides. The most important and positive aspect of this relationship is that some of these nanomaterials can be synthesized to display structures of highly reactive ceramic powders, namely small grain size in the nanometer range, narrow particle size distribution, low agglomeration tendency, regular (round) particle shape, high purity, and compositional homogeneity [1–3].

Nickel ferrite spinel belongs to a special class of magnetic materials developed for a wide range of engineering applications like magnetic devices, switching devices, microwave absorbers, active components of ferrofluids, permanent magnets, color imaging, magnetic refrigeration, biomedicine, drug delivery, magnetic resonance imaging

(MRI), anti-cancer drugs, magnetic cell separation, and catalysis [2–10].

The general formula of members of the spinel group is  $AB_2O_4$ . In a spinel structure, the anions are arranged in a cubic close-packed array with the cations in the holes. There are eight tetrahedral holes and four octahedral holes per molecule. In the case of normal spinels, the  $A^{2+}$  ions inhabit tetrahedral holes and  $B^{3+}$  ions inhabit the octahedral holes. The spinel structure incorporates many cation species of different valence states into its octahedral (B) sites and tetrahedral (A) sites to improve its stability, resulting in spinels with a wide range of characteristic temperatures, pressures, and compositions [4]. Nickel ferrite ( $NiFe_2O_4$ ) is a transition metal oxide (TMO) that has an inverse spinel structure and exhibits semiconducting properties. It is also ferromagnetic as a result of the parallel spin arrangement of  $Fe^{3+}$  ions at the tetrahedral sites and both  $Ni^{2+}$  and  $Fe^{3+}$  ions at the octahedral sites [5].

Various preparation routes have been proposed for the synthesis of nickel ferrite, including the hydrothermal approach, solvothermal approach [6], use of microemulsions [7], method of thermal decomposition, combustion, method of chemical co-precipitation [8], and the sol-gel method [9]. In particular, the sol-gel method has attracted much attention for the preparation of nickel ferrite, where the constituents are mixed on an atomic scale to uniformly distribute the active metals on the support [10]. Nowadays, microwaves are used as a heating source for the combustion reaction because of its fast-reaction kinetics, cleanliness, and efficiency, as well as the economic aspects of the process, such as cost reduction in terms of energy and time [11]. Depending on the preparation method as well as the particle size and shape, nickel ferrite exhibits different kinds of magnetic properties, such as, paramagnetic, super paramagnetic, or ferromagnetic behavior. It also exhibits unusual physical and chemical properties when its size is reduced to the nanometer scale.

The synthesis of nickel ferrite is commonly measured by an external magnetic field, and it is an effective method for preparing magnetic materials. An analysis of the effect of the distribution of magnetic lines of force on the growth of magnetic materials offers an opportunity to gain a deep understanding of the mechanism of crystal growth under the control of an external magnetic field; it also helps to determine the optimal field strength for the fabrication of magnetic materials. The self-generated magnetic field of attracted Ni crystals is expected to be responsible for the variations in their shape. The delivery of external magnetic lines of force and the self-generated magnetic field of ferromagnetic materials should be taken into account when ferromagnetic materials are fabricated in the presence of an external magnetic field.

In the present study, multifunctional  $NiFe_2O_4$  was prepared by using oxalic acid as the fuel in the sol-gel method (SGM) and the microwave method (MM). The synthesized  $NiFe_2O_4$  was characterized by powder x-ray diffraction (XRD), high-resolution scanning electron microscopy (HR-SEM), transmission electron microscopy (TEM), high-resolution transmission electron microscopy (HR-TEM), ultraviolet-visible (UV-Vis) diffuse reflectance spectroscopy, photoluminescence (PL) spectroscopy, and vibrating sample magnetometry (VSM). The results are reported and discussed in the following sections.

## 2 Experimental Section

### 2.1 Synthesis of $NiFe_2O_4$ by SGM and MM

All the chemicals used in this study were of analytical grade. They were purchased from Aldrich, India, and were used as received without further purification. Ferric nitrate ( $Fe(NO_3)_3 \cdot 9H_2O$ , 98%) and nickel nitrate ( $Ni(NO_3)_2 \cdot 3H_2O$ , 98%) were used as the starting materials, and oxalic acid was used as the fuel in the sol-gel and microwave methods. For the stoichiometric reaction between oxalic acid and the metal nitrates, reactions and the starting materials counting stoichiometric amounts (Fe/Ni = 2:1 ratio) for ferric nitrate (4.82 g), nickel nitrate (2.97 g), and oxalic acid (4.5 g) quantity used. Nickel nitrate and ferric nitrate were first dissolved in deionized water and then mixed with an oxalic acid solution under constant stirring for 3 h at room temperature until a clear transparent solution was obtained. The molar ratio of Ni/Fe was kept at 1:2. The solution was dried in an air oven at 120 °C for 1 h. The powder was then heated in a muffle furnace at a rate of 5 °C/min and then sintered at 600 °C for 3 h; hereafter, this sample, prepared by SGM, is referred to as sample A. Alternatively, the clear transparent solution was placed in a domestic microwave oven (2.45 GHz, 900 W) for 10 min. Initially, the solution boiled and underwent dehydration followed by decomposition with the evolution of gases. The solution eventually vaporized and the remaining contents became a solid; hereafter, this sample, prepared by MM, is referred to as sample B.

### 2.2 Characterization of $NiFe_2O_4$

The structural information of the synthesized nickel ferrite was obtained with an x-ray diffractometer (D<sub>8</sub> Advance, Bruker, Germany) at a wavelength of 1.54 Å. The microstructural characteristics, such as the morphology, particle size, and crystal structure of the samples were analyzed by a high-resolution scanning electron microscope (Quanta FEG200, FEI, USA). The diffuse reflectance

UV–Vis spectra of the nanomaterials were recorded by a UV–Vis spectrophotometer (Cary100UV–Visible, Agilent, USA). The emission spectra were recorded by a fluorescence spectrophotometer (Eclipse, Varian Cary, Agilent, USA). The magnetic measurements were carried out with a vibrating sample magnetometer (VSM; JDM-13, Lake Shore Cryotronics, Inc., USA) at room temperature.

### 2.3 Catalytic Reactions

Following typical procedures for aerobic oxidation of benzyl alcohol (1 mmol) in acetonitrile as the medium, the supported nickel ferrite (1 mol%) was added as a catalyst. The reaction mixture was stirred at 80 °C under 1 atm of O<sub>2</sub> (O<sub>2</sub> bubbling rate 20 ml min<sup>-1</sup>), which served as the oxidant. Upon completion of the reaction, the catalyst particles were removed from the solution by filtration. The oxidized products after the catalytic reaction were collected and analyzed with a gas chromatography (GC) spectrometer (Agilent, USA). The column used for the study was a DB-wax column (capillary column) with length of 30 mm, and helium was used as the carrier gas.

## 3 Results and Discussion

### 3.1 Structure Analysis

The phase and the crystallinity of the synthesized samples (A and B) were investigated by obtaining their x-ray diffraction patterns, shown in Fig. 1. The peaks observed at  $2\theta = 31.35^\circ, 36.94^\circ, 44.90^\circ, 55.69^\circ, 59.48^\circ,$  and  $65.25^\circ$  can be indexed to the (220), (311), (400), (422), (511), and (440) crystal planes of the cubic phase of NiFe<sub>2</sub>O<sub>4</sub>; the patterns are in good agreement with the pattern for standard cubic spinel-type NiFe<sub>2</sub>O<sub>4</sub> (JCPDS card no. 10-03250). No peaks corresponding to impurities were observed in the XRD patterns, thus demonstrating the high purity of all the oxidation products. The XRD patterns show that the peaks became narrower with longer reaction times, indicating that the crystallite size increased. However, when the reaction time was short, the nanoparticle crystallite size was very small. The calculated lattice parameter was 8.342 Å for NiFe<sub>2</sub>O<sub>4</sub>.

The average crystallite size was obtained from the XRD peaks using the Scherrer equation [12]:

$$L = \frac{0.89\lambda}{\beta \cos \theta}$$

where  $L$  is the average crystallite size (Å),  $\lambda$  is the wavelength of the incident x-ray beam (1.54 Å),  $\beta$  is the full width at half maximum (FWHM) (rad), and  $\theta$  is the Bragg angle. The average crystallite size was 23.98 and 19.76 nm for samples A and B, respectively. The ferrite peaks in

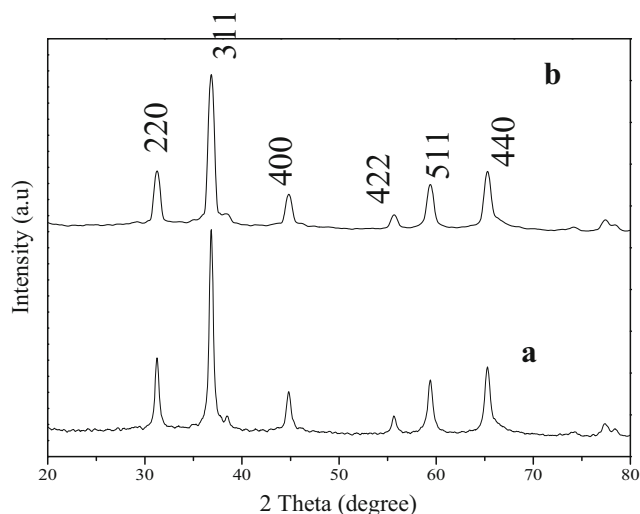


**Fig. 1** XRD pattern of **a** NiFe<sub>2</sub>O<sub>4</sub> sample A prepared by sol–gel method and **b** NiFe<sub>2</sub>O<sub>4</sub> sample B prepared by microwave method

Fig. 1 are quite broad because the crystallite domains were on the nanometer scale. The NiFe<sub>2</sub>O<sub>4</sub> peaks indicate that the size of the product decreased with increasing NiFe<sub>2</sub>O<sub>4</sub> content under the same reaction conditions. Depending on the preparation method, the Ni content affected the relative rate of nucleation and crystal growth by accelerating the nucleation rate or decelerating the crystal growth [13].

### 3.2 High-Resolution Scanning Electron Microscope Studies

The surface morphology of NiFe<sub>2</sub>O<sub>4</sub> was investigated by SEM. The NiFe<sub>2</sub>O<sub>4</sub> particles in sample A were found to have an almost spherical morphology, as shown in Fig. 2a. Figure 2b shows the formation of NiFe<sub>2</sub>O<sub>4</sub> nanoparticles in sample B, demonstrating that the molar ratio of oxalic acid played an important role in shaping the crystal structure and the morphology. The selective binding of oxalic acid to the crystal surface as a function of the surface energy controlled the morphology of the ferrite nanocrystals. Small changes in particle size were observed in the XRD and HR-SEM results, which may indicate some structural disorder and strain in the lattice caused by the different ionic radii or clustering among the nanomaterials (or a combination of different ionic radii and clustering) [14]. The samples were coated with gold by a gold-sputtering device for the better visibility of the surface morphology. The EDX result showed (Fig. 2c, d) the presence of NiFe<sub>2</sub>O<sub>4</sub> by the appearance of Ni, Fe, and O peaks in the spectrum.

### 3.3 Diffuse Reflectance Spectral Studies

Diffuse reflectance spectral (DRS) studies in the UV–Vis region were carried out to estimate the optical band gap of

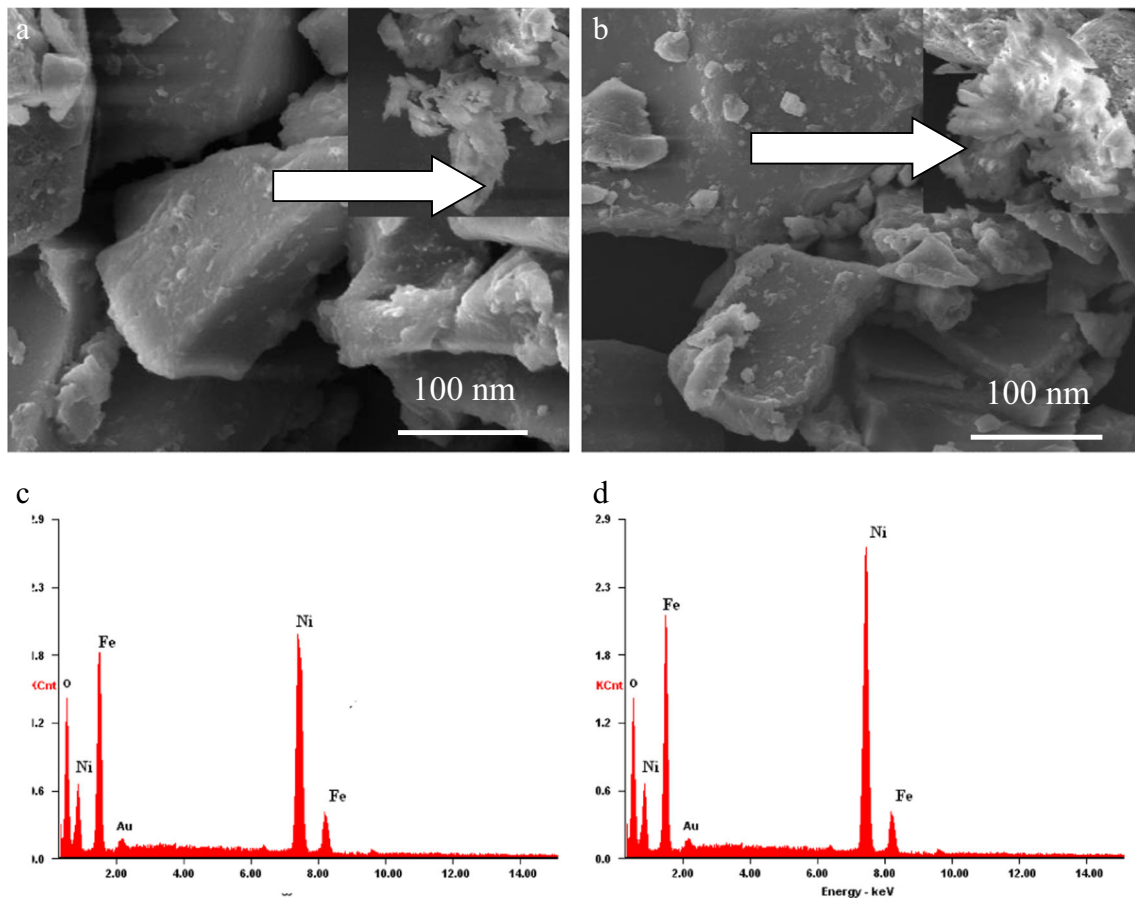


**Fig. 2** HR-SEM images of **a** NiFe<sub>2</sub>O<sub>4</sub> sample A prepared by sol-gel method and **b** NiFe<sub>2</sub>O<sub>4</sub> sample B prepared by microwave method. EDX spectra images of **c** NiFe<sub>2</sub>O<sub>4</sub> sample A prepared by sol-gel method and **d** NiFe<sub>2</sub>O<sub>4</sub>-sample B prepared by microwave method

the synthesized NiFe<sub>2</sub>O<sub>4</sub> nanoparticles in shown in Fig. 3. These results are in contrast to the projected octahedral and tetrahedral occupancy of the nickel ferrite. It is well known that the ratio of octahedral coordinated Ni<sup>2+</sup> to tetrahedral coordinated Ni<sup>2+</sup> depends on the groundwork method. Therefore, UV-DRS measurement can be a useful tool for investigating the communication of NiFe<sub>2</sub>O<sub>4</sub> nanoparticles with the supporting structure [15]. The DRS spectrum shows a NiFe<sub>2</sub>O<sub>4</sub> band and a high number of bands that probably arose from the presence of nickel species in both the octahedral and tetrahedral coordination sites. The F(R) curves of nickel ferrite are characterized by a broad band in the range of 400–550 nm and multiple bands centered in the range of 600–650 nm. Ni(II) ions with the electron configuration of 3d<sup>8</sup> have three spin-allowed electronic transitions and two spin-forbidden transitions in the UV-Vis range. Since the bands for nickel in the octahedral coordination sites correspond to higher energy than those for nickel in the tetrahedral sites, the modification can be attributed to the decrease in bands of nickel ions in the octahedral sites. Furthermore, the broadening of bands

representing the octahedral and tetrahedral sites occupied by the nickel species depended on the method used to prepare the nanoparticles (SGM or MM).

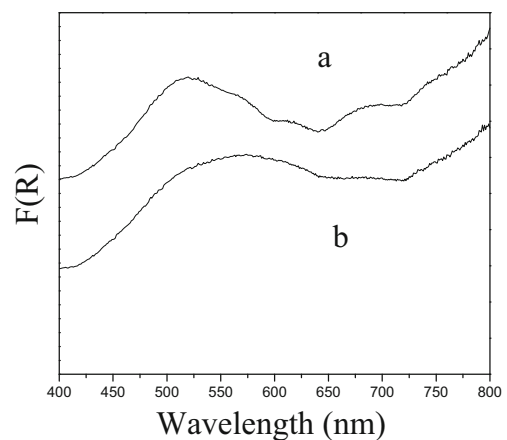


**Fig. 3** Diffuse reflectance spectra of **a** NiFe<sub>2</sub>O<sub>4</sub> sample A prepared by sol-gel method and **b** NiFe<sub>2</sub>O<sub>4</sub> sample B prepared by microwave method

### 3.4 Photoluminescence Spectra

Since the PL spectra of materials provide information on the impurities and defect energy states, they are useful for examining defect structures in semiconducting materials. Moreover, because there is considerable cation disorder in the spinel structure, there are many defects, which can serve as electron or hole traps. These defects may act as quenching centers of luminescence.

The excitation spectra can exhibit a similar degree of enhancement in intensity because of the charge-compensating ions, which are responsible for the formation of cations and oxygen vacancies. Any enhancement in luminescence observed in the PL spectra can occur for several reasons, such as energy transfer or decreased formation of charge-compensating cation vacancies or oxygen vacancies. For the nickel ferrite in our study, the PL peak positions and any increase in relative excitation intensities were examined [16].

In our study, the PL spectra features of nickel ferrite were the result of its spinel structure. Upon excitation at 325 nm, the nickel ferrite nanoparticles showed intrinsic emission peaks in the range of 480–550 nm (Fig. 4a, b). In general, nickel ferrite shows strong violet (400–450 nm), blue (450–490 nm), green (490–560 nm), yellow (560–590 nm), orange (590–635 nm), and red (635–700 nm) emission bands in the visible region. Moreover, the nature of the PL spectrum of nickel ferrite spinel depends on the method of its preparation [17, 18]. In Fig. 4, the emission spectra of NiFe<sub>2</sub>O<sub>4</sub> nanoparticles show sharp bands assigned to charge transfer between Fe<sup>3+</sup> at octahedral sites and its surrounding O<sup>2-</sup> ions. The PL spectra peak centered at 530 nm originates from near-band-gap emission, whereas the emission peak at 520–560 nm is attributed to recombination of photo-generated holes with ionized charge species from oxygen vacancies and the nickel interstitials. Hence, the blue-green emission can be attributed to the electron transition from the deep donor level of oxygen vacancies to the valence band. The defect-related (or intrinsic) emissions were different from the emissions from activated ions because the transition from the conduction band to the acceptor band (defect-related) or the transition from the donor band (defect-related) to the valence band could be affected by the micromagnetic field, while the green emission originated from the NiFe<sub>2</sub>O<sub>4</sub> nanoparticles [19].

### 3.5 Vibrating-Sample Magnetometry Measurements

The magnetic properties of the NiFe<sub>2</sub>O<sub>4</sub> samples (A and B) were recorded by a VSM at room temperature with an applied field of up to  $\pm 10$  kOe. The results shown in Fig. 5 clearly indicate that the prepared samples could be separated

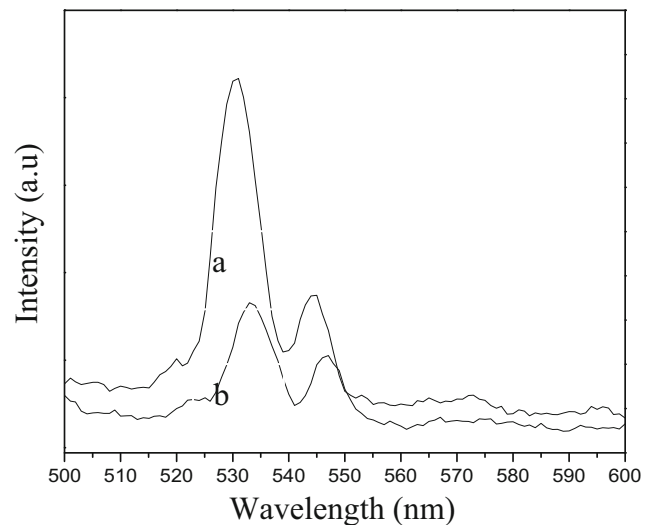


**Fig. 4** Photoluminescence spectra of **a** NiFe<sub>2</sub>O<sub>4</sub> sample A prepared by sol-gel method and **b** NiFe<sub>2</sub>O<sub>4</sub> sample B prepared by microwave method

from water via the application of the external magnetic field. The VSM results of saturation magnetization (*M<sub>s</sub>*), remanent magnetization (*M<sub>r</sub>*), and the coercivity (*H<sub>c</sub>*) are summarized in Table 1. The magnetic hysteresis (*M*–*H*) loop shows that both samples exhibited ferromagnetic behavior. Magnetic anisotropy is an important factor in ferromagnetic properties. We found that the magnetic properties depended on the structure and size of the nickel ferrite particles. More importantly, the values of *M<sub>s</sub>*, *M<sub>r</sub>*, and *H<sub>c</sub>* and the particle morphology clearly depended on the type of precursor used in the preparation of the particles. In the present study, the magnetic nanoparticles were readily distributed over the entire space and had a certain size distribution; even the total anisotropy energy barrier was distributed over a certain range. The blocking temperature and the anisotropy constant were measured for the entire nanoparticle ensemble, and the mean values must be considered. In some cases, the magnetic field controlled the preferred direction of the magnetic atoms' motion, subsequently assisting particle growth in that direction. In addition, the direct magnetic interactions between the particles were more substantial and they also played a crucial role in the morphology and size of the particles.

This mechanism indicates that the Ni crystals performed a favor by producing sideway external magnetic lines of force via a multiple-step procedure regardless of the span of the external magnetic lines of force. Nevertheless, this method could be controlled by the self-generated magnetic field of the Ni crystals. A parallel external magnetic field was optimal for obtaining high-quality Ni nanoparticles. This assembly procedure was dominated by the external magnetic field, which was controlled by the self-generated magnetic field of the quasi one-dimensional magnets in

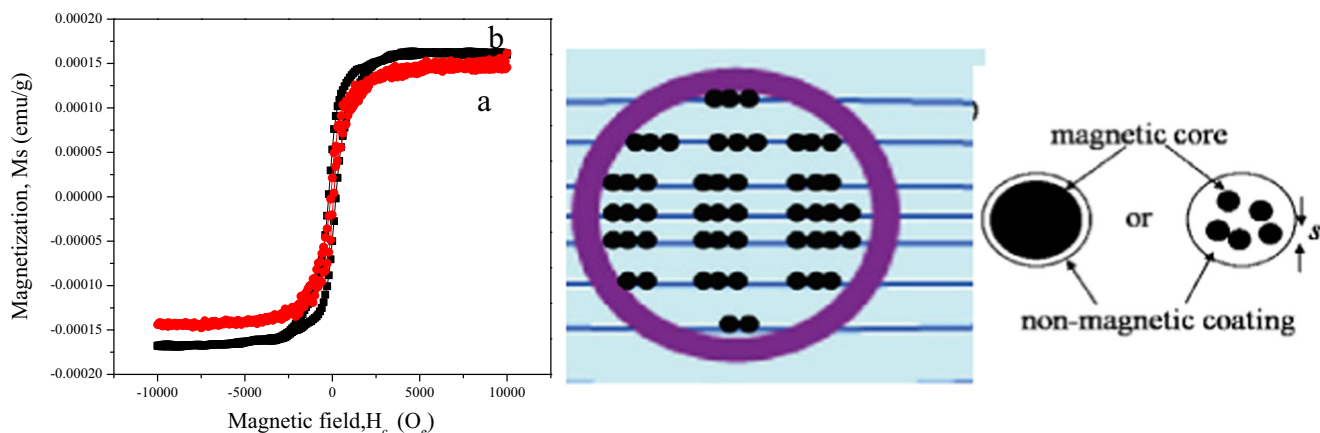


**Fig. 5** Magnetization curves of **a** NiFe<sub>2</sub>O<sub>4</sub> sample A prepared by sol-gel method and **b** NiFe<sub>2</sub>O<sub>4</sub> sample B prepared by microwave method

regions where the external magnetic lines of force were parallel lines. The external magnetic field intensity significantly affected the velocity of nucleation and growth of the ferromagnetic nanoparticles [20].

### 3.6 Selective Aerobic Oxidation of Alcohols

The catalytic oxidation of benzyl alcohol was employed as a model reaction for investigating the performance of nickel ferrite (samples A and B) as a catalyst. A comparison of the surface properties of nanocrystalline nickel ferrite samples prepared by SGM (sample A) and MM (sample B) and their oxidation activity to convert benzyl alcohol to benzaldehyde provided the following information. The catalytic studies showed that the preparation technique had a strong impact on both the conversion and product selectivity. The conversion of benzyl alcohol reached a maximum (77%) in sample B with 100% selectivity, whereas the conversion was only 51% in sample A. Sample B exhibited much stronger catalytic activity because it had higher porosity and smaller crystallite size.

### 3.7 Determination of Concentration Nickel Ferrite

In wide-ranging applicability of the relation of nanoparticle extinction coefficient versus nanoparticle size, one container use that the extinction coefficient-core diameter double logarithm curve established in this study is a calibration

**Table 1** Observed XRD and VSM data of the nickel ferrites sample (A and B) prepared by sol-gel method and microwave method

Sample	Crystallite size (nm)	Coercivity (G)	Retentivity (emu/g)	Magnetization (emu/g)
A	23.98	173.98	17.78	50.12
B	19.76	201.56	19.39	59.33

curve to calculate or estimate the nanoparticle concentration or average diameter of a nanoparticle solution sample. In the present study, the average size for nanoparticle sample is determined by using TEM, which can attain the extinction coefficient of the sample. Through capturing UV–Vis absorption spectra of the sample, the concentration of the sample can be calculated.

The concentration of nickel ferrite (mixture solution) nanoparticles was determined by the method which has been before conveyed designed for Liu et al. [21] for the gold nanoparticles. The calculation is as follows

$$N = \frac{\pi \rho D^3}{6M} N_A$$

where  $N$  is the number of atoms per nanoparticles,  $\pi = 3.14$ ,  $\rho$  is the density of face centered, cubic (fcc) nickel ferrite ( $20.5 \text{ g cm}^{-3}$ ),  $D$  is the average diameter of nanoparticles ( $40 \text{ nm} = 40 \times 10^{-7} \text{ cm}$ ),  $M$  is the atomic mass of nickel ferrite ( $130.0462 \text{ g}$ ),  $N_A$  is the number of atoms per mole (Avogadro's number) ( $6.023 \times 10^{23}$ ).

Consequently, presumptuous 100% translation of all nickel ferrite ions to nickel ferrite nanoparticles,

$$N = \frac{3.14 \times 20.5 \times 40 \times 10^{-7} \times 6.023 \times 10^{23}}{6 \times 130.0462}$$

$$N = 1987501.416163384$$

The particle size transformation in the gained standards of the particle size of NiFe<sub>2</sub>O<sub>4</sub> nanoparticles owed to the fact that the SEM or TEM (10–25 and 10–20 nm), measurements are based on the difference between the visible grain boundaries, nickel ferrite nanoparticles, concentration ions determinate for 1987501.416163384.

The average number of NiFe<sub>2</sub>O<sub>4</sub> atoms per nanoparticle might be considered from high-resolution SEM analysis. The SEM images of four nanoparticle creations were produced in this study. Through that, by using SEM ImageJ software, the average core diameters of the particles ( $D$ , nm)

were measured. This might be a main identical influential instrument for the discovery of biomarker particles by the use of a simple spectrophotometer. In addition, if the concentration and the extinction coefficient of a nanoparticle sample can be determined, the size of the particle could be estimated without imaging investigation by SEM [22].

#### 4 Conclusions

Mono-dispersed NiFe<sub>2</sub>O<sub>4</sub> nanoparticles were prepared by the sol–gel and microwave methods and the sizes of the nanoparticles were controlled by changing the reaction time. This resulted in the formation of nanoparticles with a narrow size distribution. The magnetic properties of the transition-metal ferrite nanoparticles were size-dependent and they were comparable to values commonly found in bulk ferrites, suggesting that particle size did not significantly affect the inversion degree of the spinel. The magnetic characterization is in agreement with the XRD, SEM, TEM, and the PL results. Our study shows that NiFe<sub>2</sub>O<sub>4</sub> nanoparticles can be prepared in a simple, cheap, and easy method that could potentially broaden their application.

**Acknowledgements** The authors are grateful to the Deanship of Scientific Research, King Saud University, for funding through Vice Deanship of Scientific Research Chairs and we thank Prof. C. Raghupathi, Dept. of Chemistry, S. R. College, Perumalpattu, for his help in catalysis studies.

**Author Contributions** T.A.S. and R.A. carried out the synthesis and characterization of materials in this study. M.S.A. and S.D. contributed to interpretation and analysis of the experimental results. All authors participated in the preparation and improvement of the manuscript.

#### Compliance with Ethical Standards

**Conflict of Interest** The authors declare that they have no competing interests.

#### References

1. Sun, Y., Xia, Y.N.: *Science* **298**, 2176–2179 (2002)
2. Puentes, V.F., Krishnan, K.M., Alivisatos, A.P.: *Science* **291**, 2115–2117 (2001)
3. Hakamada, M., Mabuchi, M.: *Nano Lett.* **6**, 882–885 (2006)
4. Pankhurst, Q.A., Connolly, J., Jones, S.K., Dobson, J.: *J. Phys. D: Appl. Phys.* **36**(13), R167–R181 (2003)
5. Jurgons, R., Seliger, C., Hilpert, A., Trahms, L., Odenbach, S., Alexiou, C.: *J. Phys. Condens. Matter* **18**, S2893–S2902 (2006)
6. Mathew, D.S., Juang, R.S.: *Chem. Eng. J.* **129**, 51–65 (2007)
7. Janghorban, K., Shokrollahi, H.: *J. Magn. Magn. Mater.* **308**, 238–242 (2007)
8. Srivastava, M., Ojha, A.K., Chaubey, S., Materny, A.: *J. Alloys Compd.* **481**, 515–519 (2009)
9. Gul, I.H., Maqsood, A.: *J. Alloys Compd.* **465**, 227–231 (2008)
10. Koseoglu, Y., Baykal, A., Toprak, M.S., Gozuak, F., Basaran, A.C., Akas, B.: *J. Alloys Compd.* **462**, 209–213 (2008)
11. Jadhav, S.D., Hankare, P.P., Patil, R.P., Sasikala, R.: *Mater. Lett.* **65**, 371–373 (2011)
12. Hankare, P.P., Patil, R.P., Jadhav, A.V., Garadkar, K.M., Sasikala, R.: *Appl. Catal. B: Environ.* **107**, 333–339 (2011)
13. O'Neill, H.St.C., Navrotsky, A.: *Am. Mineral.* **68**, 181–194 (1983)
14. Morrison, A.H., Haneda, K.: *J. Appl. Phys.* **52**, 2496–2498 (1981)
15. Pillai, V., Shah, D.O.: *J. Magn. Magn. Mater.* **163**, 243–248 (1996)
16. Cabuil, V., Dupuis, V., Talbot, D., Naveu, S.: *J. Magn. Magn. Mater.* **323**, 1238–1241 (2011)
17. Cheng, F., Peng, Z., Liao, C., Xu, Z., Geo, S., Yan, C., Wang, D.: *Solid State Commun.* **107**(9), 471–476 (1998)
18. Lopez, T., Alvarez, M., Gómez, R., Aguilar, D.H., Quintana, P.: *J. Sol-Gel Sci. Technol.* **33**, 93–97 (2005)
19. Mahmoud, M.H., Elshahawy, A.M., Makhlof, S.A., Hamdeh, H.H.: *J. Magn. Magn. Mater.* **343**, 21–26 (2013)
20. Lee, M.K., Kim, T.G., Ju, B.K., Sung, Y.M.: *Growth Des.* **9**, 938–941 (2009)
21. Liu, X., Atwater, M., Wang, Q., Huo, J.: *Colloid Surf. B: Biointerfaces* **58**, 3–7 (2007)
22. Maxwell, D.J., Taylor, J.R., Nie, S.: *J. Am. Chem. Soc.* **124**, 9606–9611 (2002)